

Increasing the intensity of an induction accelerator and reduction of the beam breakup instability

J. E. Coleman, D. C. Moir, C. A. Ekdahl, J. B. Johnson, B. T. McCuistian,
G. W. Sullivan, and M. T. Crawford

Los Alamos National Laboratory, Los Alamos, New Mexico 87545, USA
(Received 9 November 2013; published 19 March 2014)

A 7 cm cathode has been deployed for use on a 3.8 MV, 80 ns (FWHM) Blumlein, to increase the extracted electron current from the nominal 1.7 to 2.9 kA. The intense relativistic electron bunch is accelerated and transported through a nested solenoid and ferrite induction core lattice consisting of 64 elements, exiting the accelerator with a nominal energy of 19.8 MeV. The principal objective of these experiments is to quantify the space-charge limitations on the beam quality, its coupling with the beam breakup (BBU) instability, and provide an independent validation of the BBU theory in a higher current regime, $I > 2$ kA. Time resolved centroid measurements indicate a reduction in BBU $> 10\times$ with simply a 50% increase in the average B-field used to transport the beam through the accelerator. A qualitative comparison of experimental and calculated results are presented, which include time resolved current density distributions, radial BBU amplitude relative to the calculated beam envelope, and frequency analyzed BBU amplitude with different accelerator lattice tunes.

DOI: 10.1103/PhysRevSTAB.17.030101

PACS numbers: 29.27.Bd, 52.59.Sa, 41.75.Ht, 29.20.Ej

I. INTRODUCTION

Relativistic electron beams used to study fundamental nuclear physics or provide intense sources of photons are challenged with instabilities to overcome when increasing the intensity of the beam [1–4]. One of particular interest is the beam breakup (BBU) instability which manifests itself as a transverse magnetic coupling to destroy the beam quality. BBU was first observed in the 1960s [5] and reported in detail by Stanford Linear Accelerator Center scientists in 1968 [6]. Shortly after its discovery, BBU was studied for the first time in detail on the Experimental Test Accelerator and Advanced Test Accelerator linear induction accelerator facilities [7–10]. A 10% reduction in beam current was observed on the Experimental Test Accelerator after acceleration through eight cells with rf oscillations on the beam envelope as large as 1 cm [7]. Initially the Advanced Test Accelerator only transported 10 kA up to 15 MeV and lost 85% of the beam current at 50 MeV for vacuum transport which was later improved upon with laser ion guiding [9,10].

BBU has also been observed in the rf linac community at CEBAF, the Jefferson Lab FEL and the KEARI facility [1,2,11,12]. References [1,2] experience multipass multi-bunch BBU due to a transverse magnetic dipole higher order mode (HOM) excited by the misaligned beam bunch as it passes through the accelerator cavity. HOM in

2.15 GHz range limited CEBAF currents $\sim 40 \mu\text{A}$. After reducing the Q of the HOM through a variation in the transport matrix, threshold currents $> 100 \mu\text{A}$ were achievable. Lower energy 352 MHz and 1.3 GHz rf cavities experience 446–520 MHz HOM limiting threshold currents to $< 10 \mu\text{A}$ [11,12]. In each case BBU is suppressed through rf beam focusing using a TE HOM thereby increasing the threshold current to > 1 mA.

The first axis of the dual-axis radiography for hydrodynamic testing (DARHT) facility is exploring the limitations of increasing the intensity of the electron beam for future radiographic capabilities. DARHT Axis-I is unique for these studies because it is relatively simple to change the size of the cathode emission size to increase or reduce the total current and therefore change the space charge of the beam while holding everything else constant. In order to effectively increase the intensity of the beam, the BBU instability must be quantitatively understood and effectively eliminated. Beam position monitors (BPMs) provided time resolved centroid and BBU measurements.

As a facility BBU was first studied at DARHT analytically in 1991 [13] and experimentally on the integrated test stand which consisted of the Axis-I injector and one cell block consisting of eight induction cells [14]. This experiment scratched the surface, because BBU grows exponentially as the number of acceleration gaps is increased. BBU has also been studied extensively on DARHT Axis-II [3,4,15] and only recently has been explored in detail on the full scale DARHT Axis-I even though the accelerator has been running since 1999. The results presented provide an independent validation of the BBU theory in a higher current regime, $I > 2$ kA, and a successful demonstration

Published by the American Physical Society under the terms of the Creative Commons Attribution 3.0 License. Further distribution of this work must maintain attribution to the author(s) and the published article's title, journal citation, and DOI.

of the reduction of BBU and full transport through 64 cells without disruption of the beam quality.

II. BEAM BREAKUP INSTABILITY

As stated above in the Introduction, BBU manifests itself as a transverse magnetic coupling to destroy the beam quality. The existing TM_{0n0} modes in the induction cell cavities interact with the misaligned beam, placing a time dependent transverse magnetic dipole kick on the beam as it passes through the acceleration gap. The time-dependent dipole kick places an rf oscillation on the beam envelope, breaking up the distribution and causing eventual loss of beam current.

The BBU growth along the accelerator is characterized by the equation below [16]:

$$\frac{\xi}{\xi_o} = \left(\frac{\gamma_o}{\gamma}\right)^{1/2} \exp(\Gamma_m), \quad (1)$$

where ξ is the measured BBU amplitude at a given location and ξ_o is the measured BBU amplitude at the entrance of the accelerator. The amplitude decreases with acceleration to 1/2 power and increases exponentially with the maximum growth factor, Γ_m :

$$\Gamma_m = \frac{1}{c} I_b N_g Z_{\perp} \left\langle \frac{1}{B} \right\rangle, \quad (2)$$

where c is the speed of light, I_b is the beam current, N_g is the number of gaps, Z_{\perp} is the transverse impedance of the induction cell cavity, and $\langle 1/B \rangle$ is the average of the inverse magnetic field strength. The transverse magnetic mode couples more strongly to the beam as the current and the number of acceleration gaps increases, increasing the rf oscillation on the beam for a fixed cell design and transverse impedance. The frequency band coupled to the beam in the measurements presented below in Sec. IV (FWHM ~ 50 MHz at 750–800 MHz) is slightly smaller compared to the modes measured with a drive rod (300–900 MHz) by

Refs. [13,21,24]. Aside from designing the cell cavity to minimize the transverse impedance, reducing the number of acceleration gaps and increasing the transport magnetic field are the only ways to vacuum transport high current beams through an accelerator.

The accuracy of the BBU measurements described below is evaluated by the time of the BBU to reach maximum Γ_m , t , and resonate the induction cell cavity:

$$t = \frac{2\Gamma_m Q}{\omega}, \quad (3)$$

where Q is the quality factor of the cavity, and ω is the radial BBU frequency. The calculated saturation time of the BBU is tabulated for the separate tunes below in Sec. IV.

III. EXPERIMENTAL SETUP

The experimental configuration used to study the BBU instability was the DARHT Axis-1 linear induction accelerator (Fig. 1). The accelerator is composed of a 4 MV Blumlein injector [17,18] and 32 Blumleins [19,20] used to drive a total of 64 induction cells (two cells per Blumlein). The linear induction accelerator is broken up into eight cell blocks consisting of eight ferrite induction cores in each cell block for a total of 64 induction cells. Each induction cell has the ability to impart 250 keV of energy into the beam for a total of 16 MeV in addition to the 3.8 MeV acquired in the diode.

A. BPMs

The transported beam current and centroid is monitored by BPMs at the end of each cell block and internal to each cell block, so there is a BPM every four cells with axial spacings between 185–224 cm. The BPMs consist of eight B-dots, or inductive monitors, oriented azimuthally every 45°. There are four position B-dots, one top and bottom for $\pm y$ measurements and one left and right for $\pm x$ measurements. There are four more oriented at 45° relative to the position B-dots that are used for current averaging over

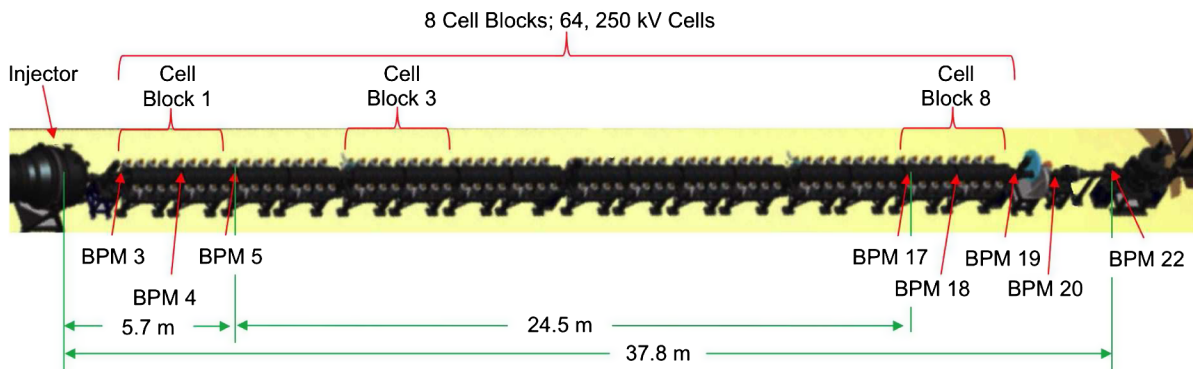


FIG. 1. Model of the DARHT Axis-I accelerator, consisting of the 4 MV injector, 64 induction cells and a BPM located after every four cells.

the cross section and as additional position measurements. The B-dots are simply a type-N coaxial feedthrough with the center conductor soldered to an aluminum tab machined out of the inner cross section of the flange they are all housed in. The B-dots pick up the inductive image current as the beam head and tail pass by the B-dot. The amplitude of the signal is dependent on the proximity of the beam relative to the B-dot. A perfectly centered beam will have equal signals on each B-dot in a BPM housing, assuming each BPM has the same impedance.

The $\pm x$ and $\pm y$ B-dots in each BPM were used to measure the BBU amplitude throughout the accelerator. This was done utilizing two methods; in the first method we used a hardware integrator (resistive and capacitive circuit) to measure the integrated position offset. This signal was normalized to the position offset in x and y and then the BBU amplitude in mm is calculated. One disadvantage of this method is the integrator effectively reduces the amplitude of the frequency spectrum. Evidence of this effect is shown below in Sec. IV where a comparison of the frequency spectrum is made between the two methods. The second method requires an unintegrated Δx and Δy signal which was sampled up to 8 GHz. A fast Fourier transform was applied to the signal over ± 50 ns in addition to the pulse length of the beam. The frequency spectrum was then integrated from 600–900 MHz to determine the BBU intensity.

B. Induction cells

The Axis-I induction cell design is described in Ref. [21]. Each cell consists of a ferrite induction core that is driven with an oil-insulated transmission line. The transverse impedance for the cells is calculated with the formula, first derived by Ref. [22],

$$\frac{Z_{\perp}}{Q} = \frac{c(\int B_y dz)^2}{2\omega_o U}, \quad (4)$$

where Q is the quality factor of the cell cavity at the resonant frequency, $B_y dz$ is transverse magnetic field component which imparts change in the transverse momentum to the particles as they traverse the acceleration gap, dz , ω_o is the resonant frequency, and U is the stored energy in the cell. This formulation indicates the importance of reducing the transverse magnetic field and damping the Q value of the resonant frequency to minimize Z_{\perp} . Another formulation of the transverse impedance from Refs. [13,21,23] with respect to the acceleration gap is

$$Z_{\perp} = Z_o \eta \frac{g}{\pi b^2}, \quad (5)$$

where Z_o is the impedance of free space (377Ω), η is a function of the surface impedance of the cavity wall, which ranges from 0.7–2, g is the accelerating gap width in the

induction cell (19 mm), and b is the beam pipe radius (73 mm) yielding $Z_{\perp} = 745.9\eta \Omega/m$, so the transverse impedance ranges from 522 to 1491 Ω/m . References [13,21,24] measured 400–1200 Ω/m over frequency ranges of 300–900 MHz on the final cell cavity design.

IV. TRANSPORT AND BBU MEASUREMENTS

The initial conditions of the beam extracted from the diode and injected into the accelerator lattice are shown in Fig. 2. The voltage in the diode is monitored by a flush mounted coaxial E-dot aligned axially with the edge of the cathode shroud. The E-dot is mounted on the surface of the vacuum tank, ~ 1 m radially from the centerline of the diode. The E-dot picks up the capacitive charge voltage as voltage rises and falls on the cathode shroud. The integrated voltage waveform is shown in Fig. 2. The extracted beam current measured at BPM02, 82.4 cm downstream of the cathode face, for the 5 cm cathode is ~ 1.7 kA and for the 7 cm cathode a current of ~ 2.9 kA is yielded (Fig. 2). The calculated beam envelope transported to the diagnostic location at $z = 167$ cm with the first transport magnet current set to 200 A is shown in Fig. 3(a) and the beam envelope transported through the diode for the 2.9 kA, 3.8 MV beam is shown in Fig. 3(b). Both envelopes were calculated using the TRAK electron-gun design code [25,26]. More details of the diode physics are described in Refs. [27,28].

We began tuning the beam envelope for the 2.9 kA beam using the nominal tune for the 1.7 kA beam and the initial envelope conditions measured from a sweep of the first transport magnet (Fig. 3). The 2 rms beam size, $a = 2\sigma$, is the second moment of the integrated $J(x, y)$ distribution from the measured optical transition radiation (OTR) profile at $z = 167$ cm [Fig. 3(c)]. The OTR measurements are taken with a 100 μm thick aluminized Kapton foil

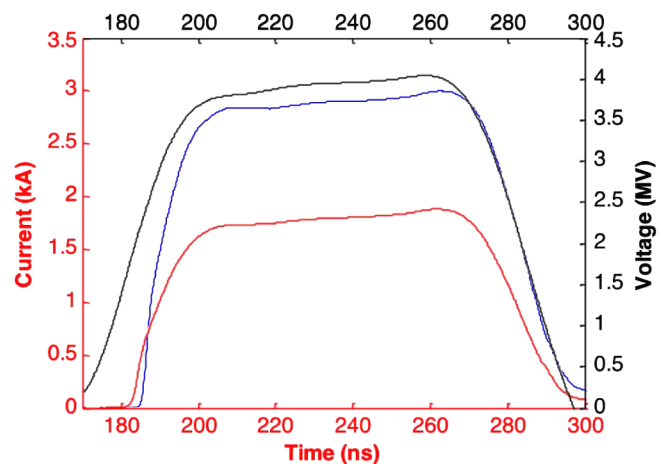


FIG. 2. Measured Blumlein voltage (black) used to extract the measured electron beam current for the 5 cm cathode (red) and the 7 cm cathode (blue). Each current was measured at BPM02, 82 cm downstream of the cathode face.

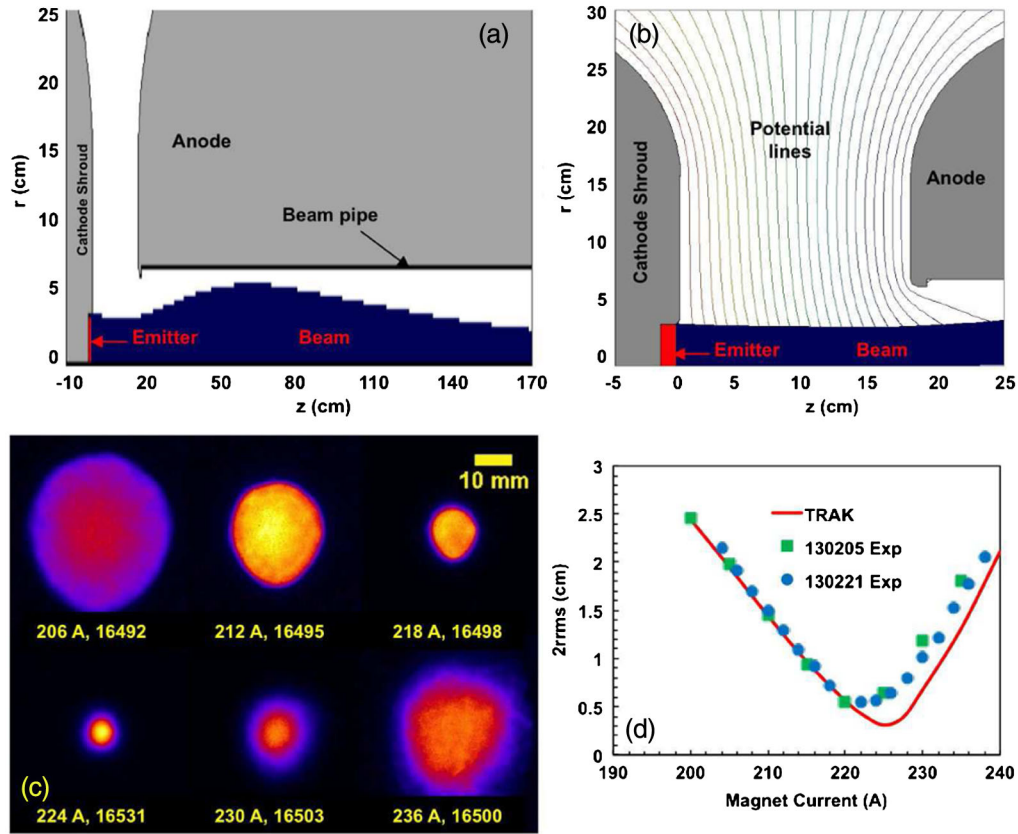


FIG. 3. (a) The transported beam envelope to the diagnostic location at $z = 167$ cm calculated in TRAK with the first transport magnet current set to 200 A; (b) the extracted beam envelope through the diode calculated in TRAK; (c) measured $J(x, y)$ for indicated transport magnet currents and shot number at $z = 167$ cm; and (d) comparison of the measured 2 rms radius of the beam and that calculated with the TRAK code at $z = 167$ cm all for the 3.8 MV, 2.9 kA beam.

target. These measurements were also compared with calculations made with the TRAK electron-gun design code and provided the initial conditions listed in Table I for transport magnet settings of 190 and 200 A. When examining Fig. 3(d) it is evident there is disagreement where the beam reaches a waist and thereafter. In the experiment the beam reaches a waist of 5.5 mm with a magnet current of 222 A (776 G); however in the TRAK calculation a slightly smaller waist of 3.1 mm is achieved with a magnet current of 225 A (787 G). However, the TRAK calculation does not include two beam-target interaction effects: the first is shorting out of the radial electric fields, which will further reduce the beam size, and the second is beam induced target heating and gas desorption [29]. The second effect will cause migrating gas desorbed off the surface of the target to be quickly ionized by the intense electron beam and the ions will backstream into the beam potential, reducing the beam space charge and overfocusing the electrons upstream of the target. This effect will increase the measured spot size at the target for magnet currents ranging from 220–230 A. When the beam on target is > 1 cm, target heating and gas desorption becomes negligible and does not explain the discrepancy in

the measured spot sizes for magnet currents > 230 A. Looking at the data more closely, it is evident that an increase in the emittance beyond the focus, due to thermalization of the beam, would explain the difference and a fit to the data indicates a 22.5% emittance growth.

We set the first magnet to 190 A for all of the tunes except our final tune. Initially it was assumed because of the high space charge ($K = 6 \times 10^{-4}$) of the beam coming out of the gun we could not converge the beam envelope too steeply because it would overfocus in the low or field-free regions between cell blocks. K is the

TABLE I. First transport magnet current, peak axial field, and initial envelope conditions at $z = 167$ cm for the 3.8 MV, 2.9 kA beam.

Current (A)	B (G)	a (mm)	a' (mrad)
190	664.45	34.96	-17.52
200	699.42	24.47	-23.41
210	734.39	14.44	-27.21
220	769.36	5.61	-23.89
230	804.33	6.76	57.88

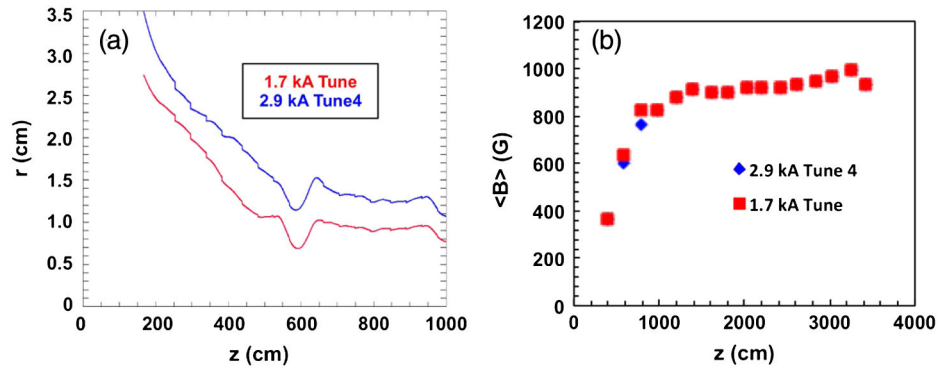


FIG. 4. (a) Calculated envelope comparison between the nominal 1.7 kA beam (red) and the first attempt at transporting the 2.9 kA beam (blue) in the first two cell blocks and (b) $\langle B \rangle$ for four cells in each cell block for both tunes.

dimensionless perveance, or the ratio of the space-charge forces to the inertial forces of the beam and is defined as

$$K = \frac{eI}{2\pi\epsilon_0 m_e (\gamma\beta c)^3}, \quad (6)$$

where e is the fundamental electron charge, I is the electron beam current, ϵ_0 is the permittivity of free space, and m_e is the electron mass. The first attempt at tuning the 2.9 kA beam, Tune 4, is shown in Fig. 4, where with a gradual increase of the magnetic field from 360 G at the beginning of the first cell block to > 800 G at the end of the second cell block we were able to gradually converge the beam envelope down to ~ 13 mm. The envelopes shown in Fig. 4(a) were calculated using the XTR code [30,31] and were initiated with the initial conditions measured and

calculated at $z = 167$ cm above in Fig. 3 and Table I. Evidence of the space-charge force quickly increasing the 2.9 kA beam radius between the cells is shown at $z = 650$ cm in Fig. 4(a). Initially only three magnets were changed in cells 8, 9, and 10 to tune the envelope of the 2.9 kA beam from the nominal 1.7 kA tune; this is evident for the $\langle B \rangle$ calculated in Fig. 4(b) where there is only a slight difference after cells 5–8 ($z = 572$ cm) and cells 9–12 ($z = 796$ cm).

After initially attempting Tune 4 and examining Eqs. (1) and (2) it was expected that the final BBU amplitude should increase by $\exp(2.9/1.7) \sim 5.5$ with everything else held constant and assuming a similar initial BBU amplitude, ξ_0 , for both cases. However, after quickly investigating the signals on the downstream BPMs it was apparent that there was a substantial amount of BBU, which manifests itself

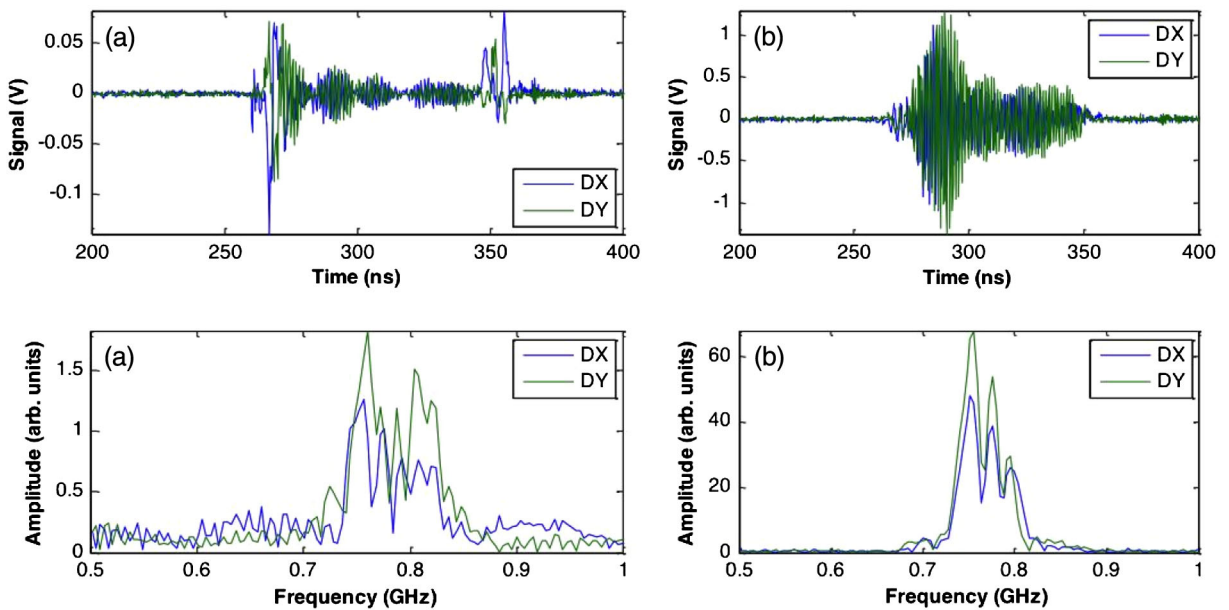


FIG. 5. Top row: Unintegrated Δx and Δy signals measured at BPM 20 ($z = 36.1$ m). Bottom row: Fast Fourier transform of the signal above to indicate the amplitude and frequency of the BBU on the beam for (a) the 1.7 kA beam and (b) Tune 4 for the 2.9 kA beam (note scale differences).

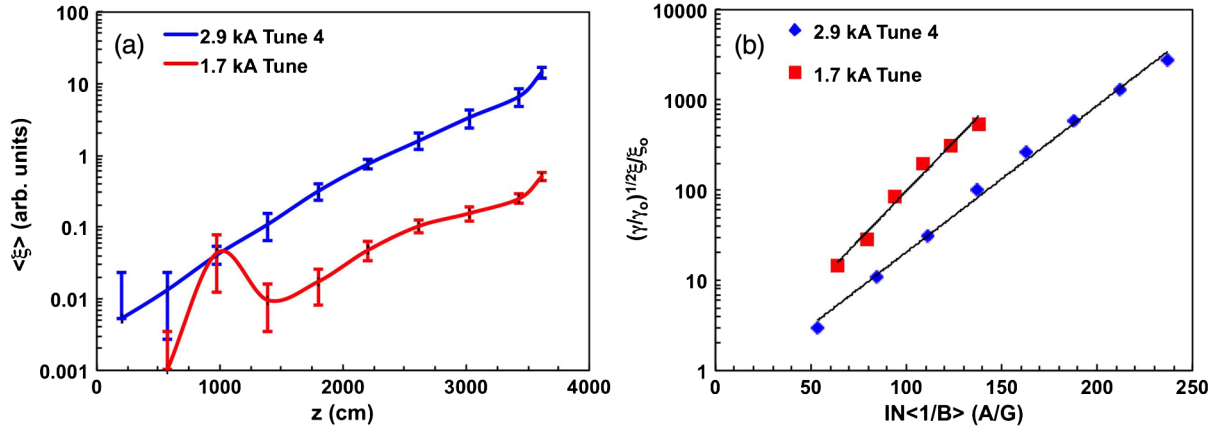


FIG. 6. (a) Increase of the average BBU amplitude $\langle \xi \rangle$ over five shots due to the increased beam current from 1.7 (red) to 2.9 kA (blue) and (b) comparison of BBU growth along the accelerator. Each tune indicates a constant transverse impedance.

as rf superimposed on the beam envelope. The top row of Fig. 5 shows the BBU on the raw signal of the 2.9 kA beam is $\sim 20\times$ higher than the 1.7 kA beam. After performing a fast Fourier transform over the 200 ns window of interest the frequency spectrum indicates nearly a $\sim 40\times$ increase in BBU. Both data sets indicate the BBU spectrum ranges from 700–850 MHz. The two cases shown here are a single shot representation for a data set composed of at least five shots; these illustrate the median BBU amplitude.

Through a more detailed analysis of the integrated frequency spectrum at the end of each cell block it is apparent that the average BBU amplitude for the 2.9 kA tune was $> 10\times$ higher than measured with the 1.7 kA beam [Fig. 6(a)]. BBU is negligible for the nominal 1.7 kA tune until BPM07 ($z = 980$ cm) and the average measured initial value for five shots is $\langle \xi \rangle = 0.044 \pm 0.032$. There is a fluctuation in the BBU amplitude along the accelerator at BPM07 for the 1.7 kA tune. This is most likely due to the coupling of a misaligned beam to the cell cavities in cell block 2 (CB2). Slight offsets > 1 mm in the beam centroid enhance the BBU amplitude. Reducing the beam centroid offsets helps mitigate the BBU growth; the physics of these effects are explored in more detail in Ref. [32]. The BBU amplitude for Tune 4 matches the 1.7 kA tune at BPM07 at the end of CB2 ($z = 980$ cm) and then increases $\sim 11\times$ the amplitude of the 1.7 kA beam at BPM09, through the third cell block. The error bars in Fig. 6(a) indicate the shot to shot variation of the BBU amplitude which ranges from 10%–60% depending on the amplitude and location. Over the length of the accelerator BBU grows $500\times$ for the 1.7 kA beam and $> 10^3\times$ for Tune 4, leading to a factor of $\sim 28\times$ higher BBU amplitude for the 2.9 kA beam at BPM 20 ($z = 3.6$ m) (Fig. 6). Direct comparison of the BBU amplitude for the 1.7 kA beam with the 2.9 kA beyond BPM07 beam clearly shows $\xi_{2.9}/\xi_{1.7} \gg \exp(2.9/1.7) \sim 5.5$. Applying a least squares fit to both data sets in Fig. 6(b) we are able to back out the slope of the exponential BBU growth and determine a

measurement of the transverse impedance of the accelerator cells. The slopes are slightly different; the 1.7 kA data set yields $1514 \Omega/\text{m}$ and the 2.9 kA data set yields $1121 \Omega/\text{m}$. Each are close to the measured and calculated cavity values mentioned above in Sec. III B.

These values for Z_{\perp} and the final $\langle B \rangle$ at the end of the accelerator lattice from Fig. 4 are used to estimate the maximum BBU growth factor, Γ_m , from Eq. (2) and are tabulated in Table II. The 1.7 kA data set yields 6.95 and the 2.9 kA data set yields 8.85, indicating $> 20\%$ increase in growth rate. The measured and calculated Q values for the induction cells from Refs. [13,14,24] range from 3–6. The saturation time of Γ_m , from Eq. (3), is calculated for the peak frequency range of the BBU amplitude (700–850 MHz). The minimum saturation time for the 2.9 kA tune, assuming $Q = 3$ and 850 MHz as the main harmonic, yields 9.9 ns and the maximum saturation time, assuming $Q = 6$ and 700 MHz, yields 24 ns (Table II). The saturation time for the 1.7 kA tune ranges from 7.8–18.9 ns. Examining the BBU signal in the top row of Fig. 5(b) we see that the BBU onset time is slightly after the beam head near 275 ns and it reaches its peak for Δx in 10 ns and its peak for Δy in 15 ns. Each of these is within the calculated saturation time for Γ_m and less than the extracted pulse length, clarifying the accuracy of these measurements.

TABLE II. Calculated transverse impedance of the Axis-I accelerator cells from a least squares fit to the BBU growth data sets for each tune. The final $\langle 1/B \rangle$, Γ_m , and the minimum and maximum saturation times for Γ_m are also tabulated.

	Z (Ω/m)	$\langle 1/B \rangle$ (1/G)	Γ_m	t_{\min} (ns)	t_{\max} (ns)
2.9 kA Tune 4	1121.2	1.28E-03	8.9	9.9	24.2
Tune 5	1088.2	1.22E-03	8.2	9.2	22.5
Tune 7	1058.3	1.17E-03	7.7	8.6	20.9
Tune 6	1079.3	1.04E-03	7.0	7.8	19.0
2.9 kA final tune	1064.3	8.55E-04	5.6	6.3	15.4
1.7 kA tune	1514.0	1.26E-03	6.9	7.8	19.0

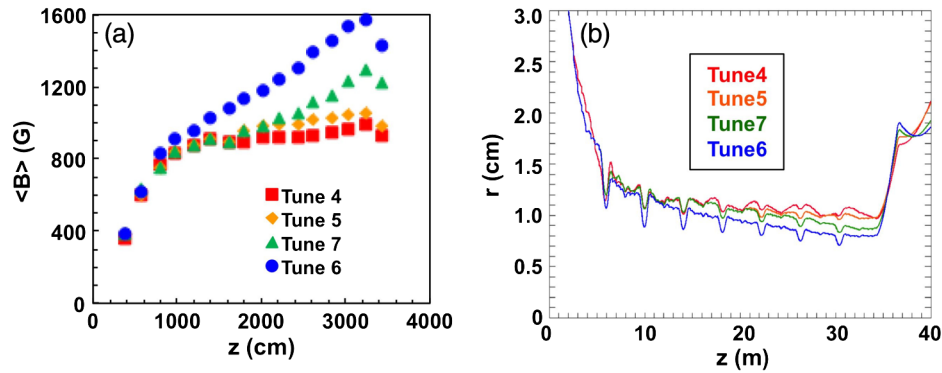


FIG. 7. (a) $\langle B \rangle$ for four cells in each cell block used reduce BBU; and (b) the reduced 2.9 kA beam envelope calculated for Tunes 4–7.

A better tune with increased $\langle B \rangle$ along the length of the accelerator was required because of this substantial growth in the BBU amplitude. The $\langle B \rangle$ in four cells of each cell block for each of the successive tunes and their corresponding envelopes calculated in XTR are shown in Fig. 7. Each tune iteration brought the beam envelope down more steeply by increasing the $\langle B \rangle$ at the end of the accelerator, where the BBU amplitude was most apparent. Eventually we had to work our way upstream and begin tuning from the first cell block, in Tune 6, because of the lack of suppression.

BBU at the upstream end of the accelerator is negligible for Tunes 5–7; it did not begin to become apparent until BPM07 ($z = 980$ cm) as shown in Fig. 8(a). A reduction in $\langle \xi \rangle$ of $\sim 5\times$ is evident at BPMs 17–20 ($z > 30$ m) in Fig. 8(a) over tune iterations from 4–6. The BBU growth along the accelerator for each successive tune is shown in Fig. 8(b). The initial BBU amplitude, ξ_o , is different for each tune contributing to the staggering of each curve. In addition the final product of $\text{IN}\langle 1/B \rangle$ decreases for each successive tune as expected, from 237 A/G for Tune 4 to 194 A/G for Tune 6; an increase in $\langle B \rangle$ of 20%. Tune 7, which has a slightly reduced $\langle B \rangle$ compared to Tune 6, is

shifted down on the BBU growth curve because its initial amplitude at BPM07, $0.0275 \gg \langle \xi \rangle$ at BPM07 for Tune 6. Each tune has nearly the same slope on the BBU growth curve [Fig. 8(b)] indicating the consistency in the transverse impedance of the induction cells in the accelerator lattice. The calculated transverse impedance for each tune, from a least squares fit to the data, is shown in Table II. The average impedance for these four tunes is $1086 \pm 26 \Omega/\text{m}$. In addition the final $\langle 1/B \rangle$, Γ_m , and the minimum and maximum saturation times for Γ_m are also included for these four tunes in Table II. It is instructive to show Γ_m is reduced 20%, indirectly proportional to the $\langle B \rangle$ increase from Tune 4 to 6. Also the saturation times for all of the tunes have an average range of 8.9–21.6 ns.

After demonstrating the ability to reduce the BBU amplitude along the accelerator and comparing results from Figs. 6 and 8 a further reduction in the BBU was required to optimize the beam quality and achieve a minimal spot size on target. For the final tune the magnetic field was increased to the highest permissible value while maintaining a constant reduction in the beam envelope without overfocusing the beam between cell blocks (Fig. 9). Initially, a higher field of 700 G (Table I) was

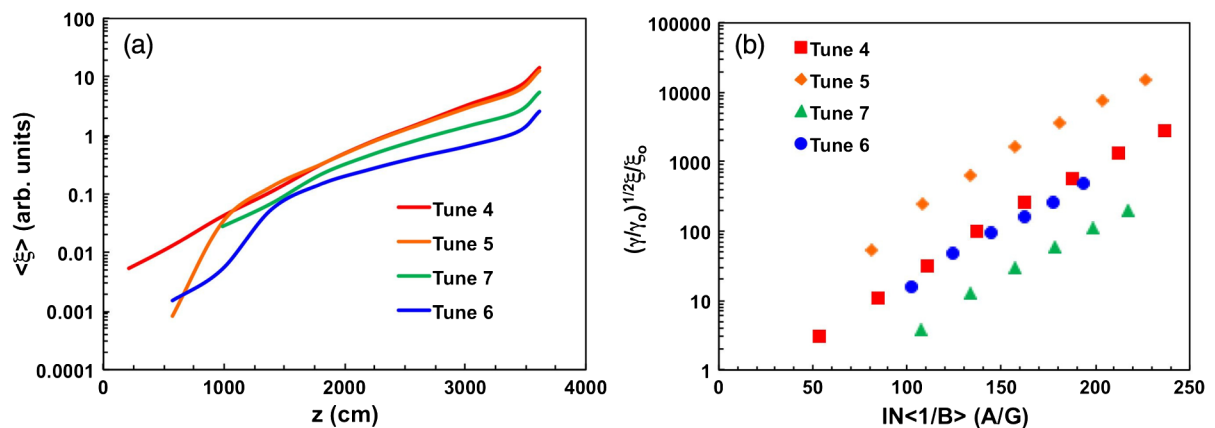


FIG. 8. (a) Reduction in the average BBU amplitude, $\langle \xi \rangle$, over five shots at each z location due to the increased $\langle B \rangle$ with each successive tune and (b) comparison of BBU growth along the accelerator for each successive tune. Each tune indicates a constant transverse impedance.

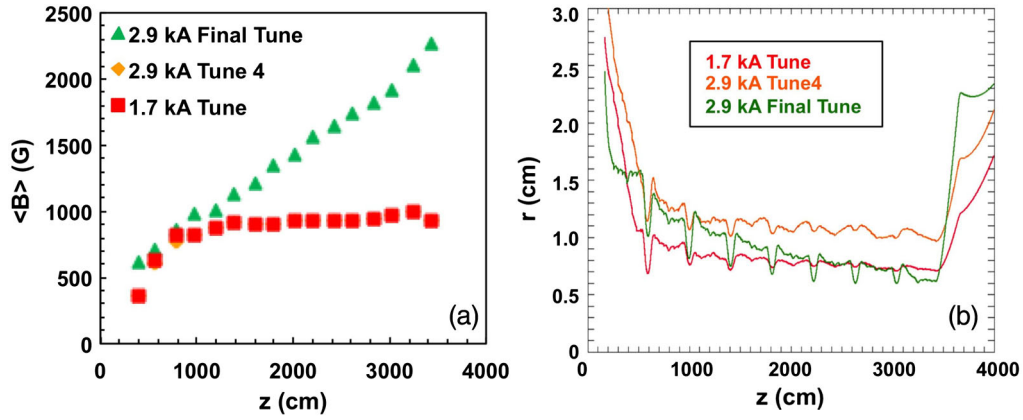


FIG. 9. (a) Plot of $\langle B \rangle$ increase from the initial 1.7 kA and final 2.9 kA tunes and (b) the corresponding calculated beam envelopes.

used for the final tune in the first transport magnet to reduce the initial radius and increase the convergence angle of the beam as it entered the first cell block as shown in envelope calculations in Fig. 9(b). The space charge of the beam made it difficult to increase the field or reduce the beam any more in size until after the second cell block ($z > 10$ m). After CB2 the field increased linearly from 1 kG up to 2.3 kG in CB8 and the beam radius was reduced from 12 to 6 mm.

This 50% increase in $\langle B \rangle$, or $2.3\times$ increase in the final field, for the 2.9 kA beam reduced $\langle \xi \rangle > 10\times$ from Tune 4 to the final tune, nearly matching the 1.7 kA tune from BPM13 ($z = 2.2$ m), end of CB5, to the end of CB8 [Fig. 10(a)]. It is worth noting the slight fluctuation in BBU amplitude at BPM07 ($z = 980$ cm) for the final 2.9 kA tune and 1.7 kA tune is due beam centroid misalignments as mentioned above. This result demonstrates the importance of increasing $\langle B \rangle$ for suppression of BBU. The 70% increase in current from 1.7 to 2.9 kA required $\sim 50\%$ increase in $\langle B \rangle$ in order to maintain relatively the same BBU amplitude. Figure 10(b) shows the relative growth of the BBU amplitude for each of the tunes. As in Fig. 8(b) the initial BBU amplitude, ξ_0 , is different for each of the tunes

in Fig. 10(b). Again a least squares fit was applied to the data sets in Fig. 10(b) and their transverse impedances are indicated in Table II. They are all slightly different, but each is near the measured and calculated cavity values mentioned above in Sec. III B. The final $\langle 1/B \rangle$, Γ_m , and minimum and maximum saturation times for these tunes are also shown in Table II; indicating a further reduction in Γ_m has been achieved with the final 2.9 kA tune and cavity saturation times < 20 ns.

The alternative method of analyzing the BBU amplitude with respect to the beam size, as mentioned in Sec. III A, was also done. However, prior to examining these results it is important to point out the comparison of the hardware integrated BPM signal versus the raw unintegrated case. This comparison was done for highest BBU amplitude tune, the 2.9 kA Tune 4, at BPM19 ($z = 34.3$ m), the end of the accelerator lattice, where the BBU amplitude was substantially large. A single shot representation, indicating the median BBU amplitude, from at least five shots of the two sampling methods is shown in the top row of Fig. 11. It is worth noting that the signal amplitude of the hardware integrated case is nearly an order of magnitude less than raw unintegrated case. A fast Fourier transform was applied

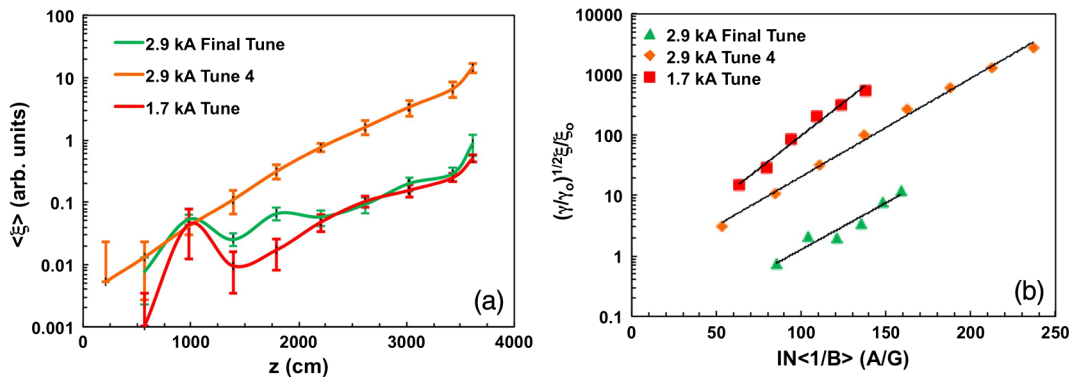


FIG. 10. Comparison of the average (a) BBU amplitude $\langle \xi \rangle$ over five shots for the 1.7 kA beam (red), initial (orange) and final 2.9 kA tunes (green) and (b) comparison of BBU growth along the accelerator. Each tune indicates a constant transverse impedance.

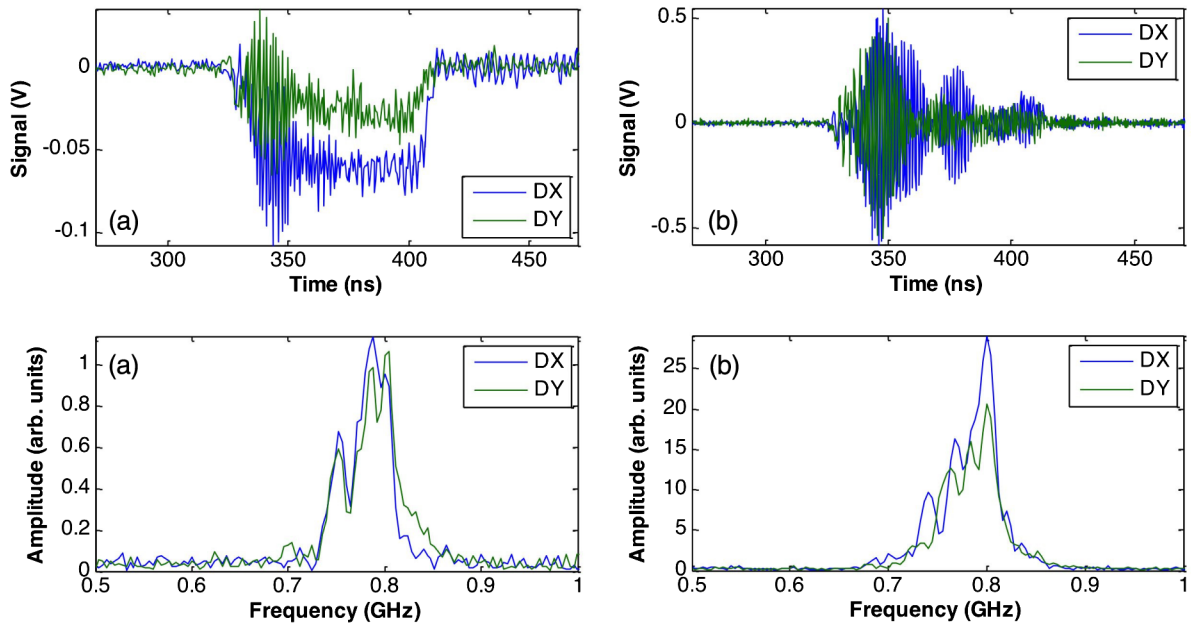


FIG. 11. Top row: Comparison of the measured (a) hardware integrated BPM signal and (b) the raw unintegrated BPM signal at BPM19 ($z = 34.3$ m). Bottom row: Fast Fourier transform of the signals above to indicate the amplitude and frequency of the BBU on the beam (note scale differences).

to the signal over ± 50 ns in addition to the pulse length of the beam for both data sets and the frequency spectrum is shown in the bottom row of Fig. 11. In both cases the frequency spectrum ranges from 700–900 MHz however the peak of the unintegrated case is $25\times$ higher. After integrating the frequency spectrum from 600–900 MHz, to determine the BBU intensity, it was evident that the $\langle \xi \rangle$ for five shots was $20\times$ higher for the unintegrated case. This indicates the sensitivity of raw unintegrated signals and the importance of using this method for the BBU analysis.

The fluctuation of the beam distribution relative to the beam size, radial BBU amplitude, was examined at the end of the accelerator lattice where the beam distribution was expanding, due to field-free transport, at BPM 22 ($z = 37.8$ m) for the tunes in Figs. 9 and 10. The 2 rms envelope for each of these tunes at BPM22 is listed in Table III and can be extracted from Fig. 9(b). After

TABLE III. Calculated 2 rms radius of the beam, a , for 1.7 kA beam, the initial, and final 2.9 kA tunes in addition to the average measured BBU amplitude (in mm) for five shots in the x and the y direction and the rms value ξ . All values pertain to BPM22, $z = 37.8$ m.

	2.9 kA Tune 4	1.7 kA tune	2.9 kA final tune
a (mm)	17.5	13	22
$\langle x \rangle$ (mm)	7.0 ± 3.7	0.35 ± 0.03	0.95 ± 0.07
$\langle y \rangle$ (mm)	4.1 ± 2.8	0.27 ± 0.03	0.49 ± 0.06
$\langle \xi \rangle$ (mm)	8.1 ± 4.6	0.44 ± 0.03	1.07 ± 0.05

normalizing out the beam centroid offsets at BPM22 the BBU motion on the beam is examined in Fig. 12. The standard deviation of the measured fluctuation of the beam distribution is calculated in x and y over the 50 ns window. A single shot representation, indicating the median BBU amplitude, from at least five shots is shown in Fig. 12. This was done for at least five shots for each tune and a tabulation of the results is shown in Table III. The BBU amplitude for Tune 4 is 8.1 ± 4.6 mm or nearly 50% of the beam size, whereas the amplitude for the 1.7 kA tune and the final 2.9 kA tune are about 3% and 5% of the beam size; indicating the importance of having $\langle \xi \rangle / a \leq 5\%$.

One additional comparison to make note of aside from the radial BBU amplitude is the beam current measured at BPM22. A clear indicator that the BBU is rf disruption on the beam distribution is to examine the beam current [Fig. 13(a)]. The beam current for the 1.7 kA tune and the final 2.9 kA tune are relatively constant throughout the beam pulse, whereas the initial 2.9 kA Tune 4 current is broken up along the pulse with rf. There is not bunching of the beam current for the 2.9 kA Tune 4, but a large rf oscillation on the beam envelope that may result in an aliasing [33]. At this z location (37.8 m) we are > 3.5 m from the nearest induction cell cavity to be picking up rf. The total charge of the two 2.9 kA tunes measured at BPM22 agrees to within 2%. The summary of the radial BBU amplitude along the length of the accelerator is shown in Fig. 13(b). It is important to point out that radial BBU amplitude as summarized in Table III is nearly an order of magnitude higher for the initial 2.9 kA Tune 4 at the end of the accelerator and begins to grow drastically after CB5,

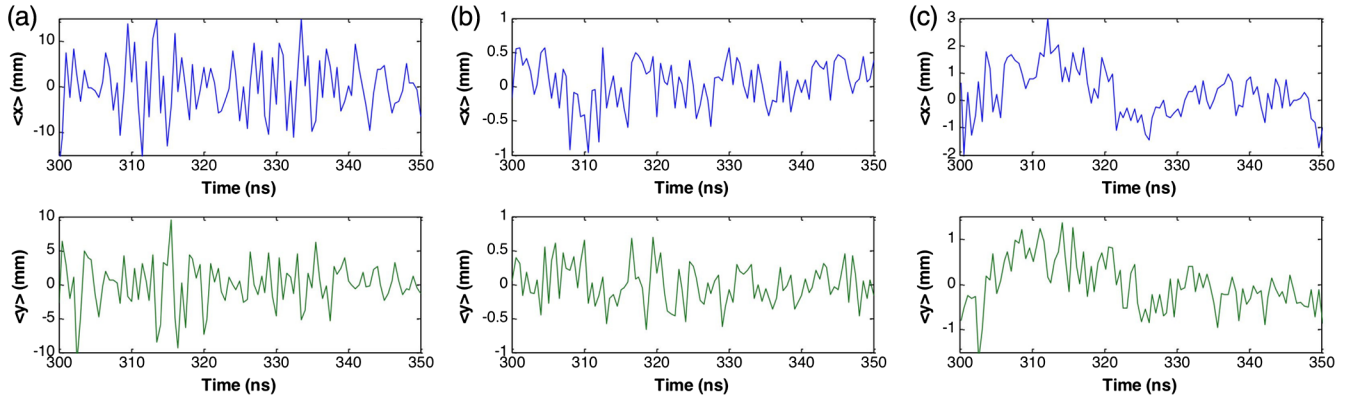


FIG. 12. Comparison of the fluctuation of the beam distribution in x and y at BPM 22 ($z = 37.8$ m) for a single shot that represents the average case for five shots for (a) the initial 2.9 kA tune 4, (b) 1.7 kA tune, and (c) the final 2.9 kA tune (note scale differences).

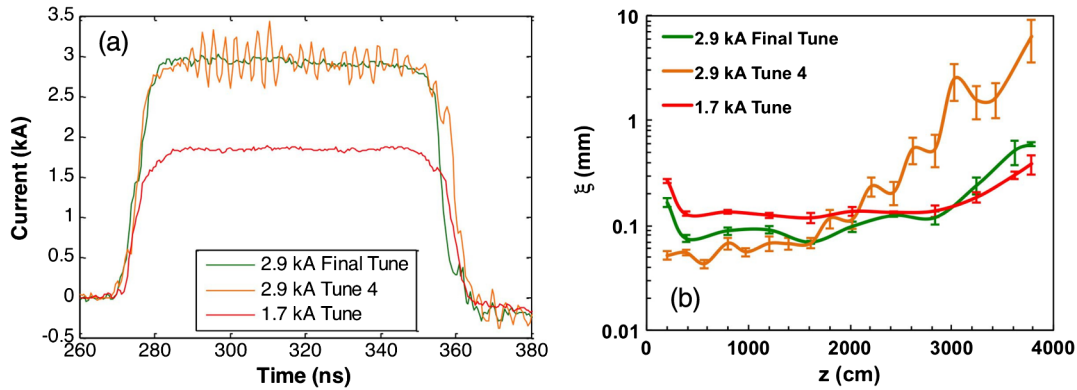


FIG. 13. Comparison of the (a) beam current measured at BPM 22 ($z = 37.8$ m) and (b) the average radial BBU amplitude in (mm) along the axis. Shot variations are indicated by error bars. Each is shown for the 1.7 kA tune (red), the initial 2.9 kA Tune 4 (orange), and the final 2.9 kA tune (green).

$z > 20$ m. The radial BBU amplitude for the 1.7 kA tune and the final 2.9 kA tune track pretty closely to one another throughout the whole accelerator. The final numbers at BPM22 in Fig. 13(b) are slightly different than in Table III because a larger data set was used for Table III.

V. CONCLUSIONS

An increase in the intensity of the DARHT Axis-I beam of 70%, with nearly the same transport lattice, leads to a $\sim 28\times$ increase in the final BBU amplitude. After several tune iterations, we successfully reduced the BBU amplitude $5\times$ by simply increasing the $\langle B \rangle$ in the accelerator 20%. However, this was still insufficient; a final tune was developed to increase $\langle B \rangle$ by 50%, or the B-field at the accelerator exit by $2.3\times$, to reduce the BBU from Tune 4 by $>10\times$, a comparable level to our nominal 1.7 kA tune.

Comparison of the unintegrated BPM measurements to the hardware integrated BPM measurements indicate a sampling sensitivity of $>20\times$ and the importance of using this method for the BBU analysis. These axially dependent BBU measurements indicate the necessity of increasing the $\langle B \rangle$ in an accelerator lattice to reduce BBU and the

difficulty of designing an accelerator lattice for an electron beam with a dimensionless perveance $> 10^{-4}$. These experiments are another independent validation of the theory in Ref. [16], Eqs. (1) and (2), as it applies to high-current linear induction accelerators with strong solenoidal fields. These results lend confidence for the use of this theory for future intense relativistic accelerator facilities, which will continue to be challenged by space-charge force limits on focusing strength combined with required B to minimize BBU.

ACKNOWLEDGMENTS

This work was supported by the National Nuclear Security Administration of the U.S. Department of Energy under Contract No. DE-AC52-06NA25396. I would like to take the opportunity to thank the DARHT Axis-I operators and technicians James Carothers, Sam Snider, Melissa Reed, Jules Carson, Tim McCurdy, Rudy Valdez, and Edward Jacquez for their continued support.

- [1] R. Kazimi *et al.*, in *Proceedings of the 11th European Particle Accelerator Conference, Genoa, 2008* (EPS-AG, Genoa, Italy, 2008), p. 2722.
- [2] C. Tennant *et al.*, in *Proceedings of FEL2004 Conference* (Comitato Conferenze Elettra, Trieste, Italy, 2004), p. 590.
- [3] C. Ekdahl *et al.*, *IEEE Trans. Plasma Sci.* **34**, 460 (2006).
- [4] C. Ekdahl *et al.*, *Phys. Rev. ST Accel. Beams* **14**, 120401 (2011).
- [5] M. G. Kelliher and R. Beadle, *Nature (London)* **187**, 1099 (1960).
- [6] W. K. H. Panofsky and M. Bander, *Rev. Sci. Instrum.* **39**, 206 (1968).
- [7] R. J. Briggs, D. L. Bix, G. J. Caporaso, T. J. Fessenden, R. E. Hester, R. Melendez, V. K. Neil, A. C. Paul, and K. W. Struve, *IEEE Trans. Nucl. Sci.* **28**, 3360 (1981).
- [8] G. J. Caporaso, A. G. Cole, and K. W. Struve, *IEEE Trans. Nucl. Sci.* **30**, 2507 (1983).
- [9] G. J. Caporaso *et al.*, in *Proceedings of the 5th International Conference on High-Power Particle Beams, San Francisco, CA, 1983*, p. 427.
- [10] G. J. Caporaso, in *Proceedings of LINAC, Stanford, CA, 1986*, p. 17.
- [11] V. Volkov, *Phys. Rev. ST Accel. Beams* **12**, 011301 (2009).
- [12] V. Volkov, J. Knobloch, and A. Matveenko, *Phys. Rev. ST Accel. Beams* **14**, 054202 (2011).
- [13] P. Allison, in *Proceedings of the 1991 Particle Accelerator Conference, San Francisco, CA, 1991* (IEEE, New York, 1991), p. 520.
- [14] P. Allison, in *Proceedings of the Particle Accelerator Conference, Vancouver, BC, Canada, 1997* (IEEE, New York, 1997), p. 1138.
- [15] Y.-J. Chen, in *Proceedings of the Particle Accelerator Conference, Chicago, IL, 2001* (IEEE, New York, 2001), p. 3490.
- [16] V. K. Neil, L. S. Hall, and R. K. Cooper, *Part. Accel.* **9**, 213 (1979).
- [17] J. Fockler, B. Bowen, V. Carboni, P. Corcoran, J. Kishi, and R. Kuenning, in *Proceedings of the 8th IEEE International Pulsed Power Conference, San Diego, CA, 1991*, p. 177.
- [18] J. Downing *et al.*, in *Proceedings of the 8th IEEE International Pulsed Power Conference, San Diego, CA, 1991*, p. 949.
- [19] N. C. Jaitly *et al.*, in *Proceedings of the 20th Power Modulator Symposium, Myrtle Beach, SC, 1992*, p. 227.
- [20] N. C. Jaitly *et al.*, in *Proceedings of the 10th IEEE International Pulsed Power Conference, Albuquerque, NM, 1995*, p. 1412.
- [21] M. Burns *et al.*, in *Proceedings of the 1991 Particle Accelerator Conference, San Francisco, CA, 1991* (Ref. [13]), p. 2958.
- [22] R. J. Briggs *et al.*, *Part. Accel.* **18**, 41 (1985).
- [23] R. J. Briggs *et al.*, in *Proceedings of the Particle Accelerator Conference, Chicago, IL, 2001* (Ref. [15]), p. 1850.
- [24] L. Walling *et al.*, in *Proceedings of the 1991 Particle Accelerator Conference, San Francisco, CA, 1991* (Ref. [13]), p. 2958.
- [25] S. Humphries, Jr., *AIP Conf. Proc.* **297**, 597 (1993).
- [26] S. Humphries, Jr., *Field Solutions on Computers* (CRC Press Boca Raton, FL, 1997); and <http://www.fieldp.com>.
- [27] J. E. Coleman, D. C. Moir, C. A. Ekdahl, J. B. Johnson, B. T. McCuistian, and M. T. Crawford, in *Proceedings of the 2013 IEEE Pulsed Power & Plasma Science Conference, San Francisco, CA, 2013*.
- [28] J. E. Coleman (unpublished).
- [29] C. Vermare, H. A. Davis, D. C. Moir, and T. P. Hughes, *Phys. Plasmas* **10**, 277 (2003).
- [30] T. P. Hughes, D. C. Moir, and P. W. Allison, in *Proceedings of the Particle Accelerator Conference, Vancouver BC, 1995*, p. 1207.
- [31] P. Allison, Report No. LA-UR-01-6585.
- [32] J. E. Coleman *et al.* (unpublished).
- [33] C. Ekdahl, *Rev. Sci. Instrum.* **76**, 095108 (2005).